High-resolution tungsten spectroscopy relevant to the diagnostic of high-temperature tokamak plasmas

High-resolution tungsten spectroscopy relevant to the diagnostic of high-temperature tokamak plasmas

J. Rzadkiewicz[3], Y. Yang[1,2], K. Kozioł[3], M G O'Mullane[4], A. Patel[5], J. Xiao[1,2], K. Yao[1,2], Y. Shen[1,2], D. Lu[1,2], R. Hutton[1,2] and Y. Zou[1,2]

[1]*The Key Laboratory of Applied Ion Beam Physics of Ministry of Education, Shanghai 200433, China*
[2]*Shanghai EBIT Laboratory, Institute of Modern Physics, Fudan University, Shanghai 200433, China*
[3]*Narodowe Centrum Badań Jądrowych (NCBJ), Andrzeja Sołtana 7, 05-400 Otwock-Swierk, Poland*
[4]*Department of Physics, University of Strathclyde, Glasgow G4 0NG, UK*
[5]*Euratom/CCFE Fusion Association, Culham Science Centre, Abingdon, OX14 3DB, UK*

The x-ray transitions in Cu- and Ni-like tungsten ions in the 5.19-5.26 Å wavelength range that are relevant as a high-temperature tokamak diagnostic, in particular for JET in the ITER-like wall configuration, have been studied. Tungsten spectra were measured at the upgraded Shanghai-EBIT operated with electron beam energies from 3.16 keV to 4.55 keV. High-resolution measurements were performed by means of a flat Si 111 crystal spectrometer equipped by CCD camera. The experimental wavelengths were determined with an accuracy of 0.3-0.4 mÅ. The wavelength of the ground states transition in Cu-like tungsten from the $3p^5 3d^{10} 4s4d\ [(3/2,(1/2,5/2)_2]_{1/2}$ level was measured for the first time. All measured wavelengths were compared with those measured from JET ITER-like wall plasmas and with other experiments and various theoretical predictions including COWAN, RELAC, MCDF and FAC calculations. In order to obtain a higher accuracy from theoretical predictions, the MCDF calculations were extended by taking into account correlation effects (configuration interaction). It was found that such an extension brings the calculations closer to the experimental values in comparison with other calculations.

I. INTRODUCTION

The study of characteristic x-ray radiation emitted by highly ionized high-Z atoms is of great importance for both theoretical and applied atomic physics including fusion applications [1-3]. Measurements of such radiation can probe strong relativistic, quantum-electrodynamics (QED) and correlation effects. Neon-like and nickel-like heavy ions were proposed for x-ray lasing emission [4,5]. In fusion application spectral analysis of mid- and high-Z atomic systems are used to obtain key plasma parameters related to the metallic impurity concentrations, ion and electron temperatures, rotation velocity and Z_{eff} [6-9].

The selection of tungsten as a plasma facing material for ITER has brought particular interest in its spectroscopic studies [10]. Recently extensive experimental studies were performed on the atomic structure and properties of x-ray transitions in tungsten, from lithiumlike W^{71+} [11] through near-neonlike W^{64+}, near-potassiumlike W^{55+} [12-15], near-nickellike W^{46+} [3,16] and near-palladiumlike W^{28+} [17,18] down to ytterbiumlike W^{4+} tungsten [19]. Measurements of impurity x-ray spectra were also performed at ASDEX Upgrade and JT60U tokamaks for highly ionized tungsten ions up to Cu-like (W^{45+}) and Na-like (W^{63+}), respectively [20,21].

The experimental spectroscopic studies of tungsten ions were intensively supported by extensive theoretical considerations (see e.g. Ref. [22] and Refs. within). In the last few years a significant improvement has been achieved in the theoretical approaches, in particular by the development of large-scale relativistic configuration interaction (CI) methods taking into account electron correlation effects. Such a technique was employed for M1 transitions in Ag-and Cd-like tungsten [18,23], electric-multipole transitions in Sn-like tungsten [24,25] and for transitions from low-lying levels in Ni-like tungsten [26]. An extended experimental and theoretical data base on the tungsten ions can be found in Refs. [27-29].

Recently, in measurements on the Joint European Torus (JET) with ITER-like wall (ILW) configuration (beryllium wall and tungsten divertor) [30, 31], the W^{45+} and W^{46+} (3p-4d) x-ray lines were observed. From analysis of tungsten line intensities, it was found that the W concentration is $\sim 10^{-5}$ for the ELMy H-mode JET plasmas with 2.0–2.5 MA current, 2.7 T toroidal magnetic field and 14–18 MW neutral beam injection (NBI) power. Measured tungsten concentrations were only consistent using the W^{46+} line not with the W^{45+} line for un-seeded low current (~2.0 MA) JET ILW plasmas [7]. It was further shown that in order to reproduce the experimental spectra in the 5.192–5.232 Å wavelength range measured for the electron temperature ~4 keV and density $\sim 3 \times 10^{19}$ m^{-3}, it is necessary to perform advanced atomic studies that include specific electron contributions for considered W ion stages, especially for those with open shells (e.g. W^{45+} and W^{47+}) [32,33].

Here we report on high-resolution measurements of Cu- and Ni-like tungsten spectra performed at the Shanghai EBIT. Spectra relevant to the high-resolution x-ray diagnostic in JET were measured in the 5.19–5.26 Å wavelength region at the energies of the electron beam from 3.16 keV to 4.55 keV and compared with those measured at JET and with theoretical spectra calculated by extensive relativistic codes: FAC, utilizing the modified Dirac-Hartree-Slater (DHS) method and GRASP2K, utilizing the Multi-Configuration Dirac-Fock (MCDF) method. In order to obtain high-accuracy theoretical predictions within the MCDF-CI method, large scale CI calculations were performed.

II. EBIT EXPERIMENT

High-resolution x-ray measurements were performed at the upgraded Shanghai-EBIT laboratory [34]. A general scheme of the experimental set-up at the upgraded Shanghai-EBIT is shown at Figure 1. Tungsten was injected into EBIT as sublimation of tungsten hexacarbonyl $W(CO)_6$ through a gas injection system into the trapping region.

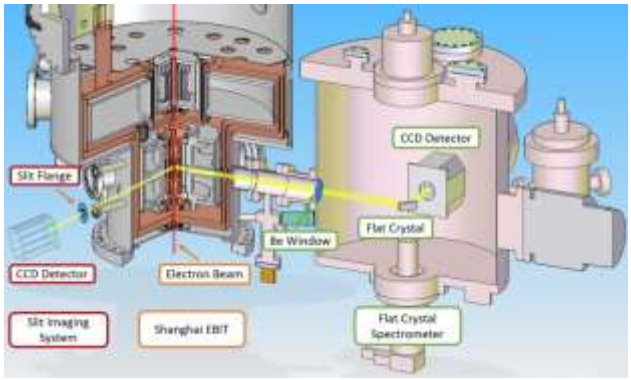

FIG. 1. A general scheme of the experimental set-up at the upgraded Shanghai-EBIT.

Highly-ionized tungsten ions were produced by an electron beam with energies from 3.16 keV to 4.55 keV, current of 15-70 mA that correspond to electron density of 2.5-11.6 x 10^{18} m^{-3}. The electron densities were determined from the measurements of the diameters of the electron beam by the slit imaging system [35] (see Fig. 1) and from accurate measurements of electron beam energy and the current. The full width at half maximum diameter of the electron beam was found to be less than 70 μm. The width of the electron beam energy distribution was ~20 eV. The magnetic field in the central trap region was about 3 T. Table I shows the Shanghai-EBIT operation parameters set for the present experiment.

The x-ray spectra were registered by the flat field spectrometer equipped with a Si111 crystal with dimensions of 5.0x2.5x0.5cm^3 and 2d=6.2712 Å [36] and charge coupled device (CCD) detector with 2048x2048 pixels (Δx=13.5 μm). The resolving power of the spectrometer was found to be not worse than λ/Δλ~4200 in the wavelength region of the investigation. The spectrometer was set to measure tungsten spectra at the wavelength range from 5.19 Å to 5.26 Å around the ~56.5° Bragg angle. Data collection times were between 22h and 86h per spectrum. Figure 2 shows tungsten spectra induced by electron beams at energies of 3.16 keV, 3.76 keV, 4.34 keV and 4.55 keV. X-ray lines appearing in the spectra are described in Table II.

Table I. EBIT electron beam parameters (current, energy and corresponding electron density).

E_e (keV)	I_e (mA)	N_e x 10^{18} (m^{-3})
3.16	15	2.5
3.76	37	6.3
4.34	38	5.1
4.55	70	11.6

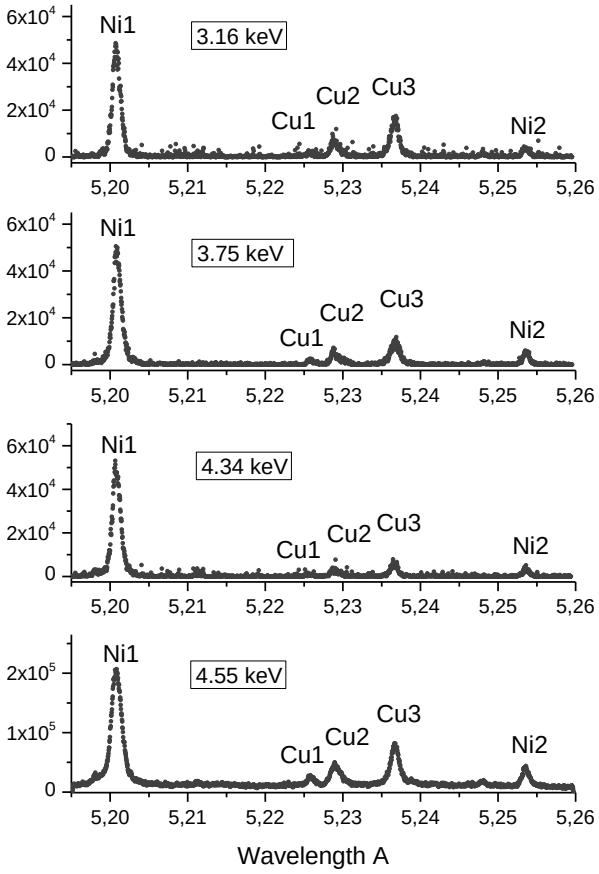

FIG. 2. X-ray spectra of Cu- and Ni-like tungsten ions measured on the upgraded Shanghai-EBIT for electron beam energies of 3.16, 3.76 and 4.34 keV.

TABLE II. X-ray lines of Ni-and Cu-like tungsten ions observed in the 5.19-5.26 Å spectral range.

Line	Upper level	Lower level
Ni1	$3p^5 3d^{10} 4d\ (3/2,5/2)_1$	$3p^6 3d^{10}\ {}^1S_0$
Cu1	$3p^5 3d^{10} 4s4d\ [(3/2,(1/2,5/2)_2]_{3/2}$	$3d^{10} 4s\ {}^2S_{1/2}$
Cu2	$3p^5 3d^{10} 4s4d\ [(3/2,(1/2,5/2)_2]_{1/2}$	$3d^{10} 4s\ {}^2S_{1/2}$
Cu3	$3p^5 3d^{10} 4s4d\ [(3/2,(1/2,5/2)_3]_{3/2}$	$3d^{10} 4s\ {}^2S_{1/2}$
Ni2	$3p^5 3d^{10} 4d\ (3/2,3/2)_1$	$3p^6 3d^{10}\ {}^1S_0$

III. JET MEASUREMENTS

The W^{45+} and W^{46+} (3p-4d) x-ray lines were observed at JET by means of an upgraded high-resolution x-ray spectrometer (KX1 diagnostic) at ~5.2 Å wavelength region [37-39]. Figure 3 shows an example of such spectrum measured from typical steady state ion cyclotron resonance frequency (ICRF) heated plasmas at JET shot #85909 between 16-17s. The corresponding electron density and temperature profiles (JET discharge # 85909, 16-17s) measured by the LIDAR Thomson scattering [40] are shown in Figure 4 (together with fitting curves). It can be seen that both, electron temperature and density profiles are almost unchanged over the considered period of time in JET discharge #85909. The profiles correspond to the average electron temperature <Te>3.9 keV and density <ne>= $3.2\times10^{19} m^{-3}$ of JET plasmas on magnetic axis.

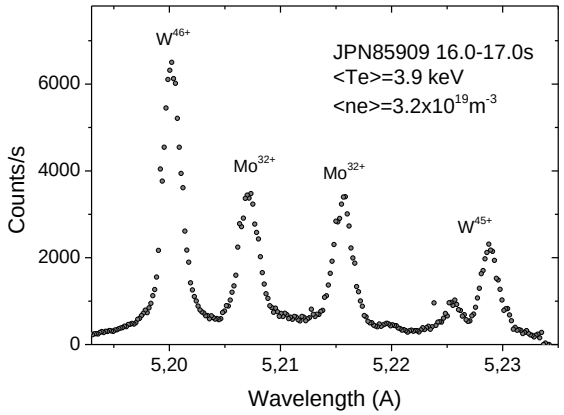

FIG. 3. Tungsten (W^{45+} and W^{46+}) and molybdenum (Mo^{32+}) x-ray lines observed in the spectrum measured at JET (shot #85909) for the $T_e \approx 3.9$keV and $n_e \approx 3.2\times10^{19}m^{-3}$.

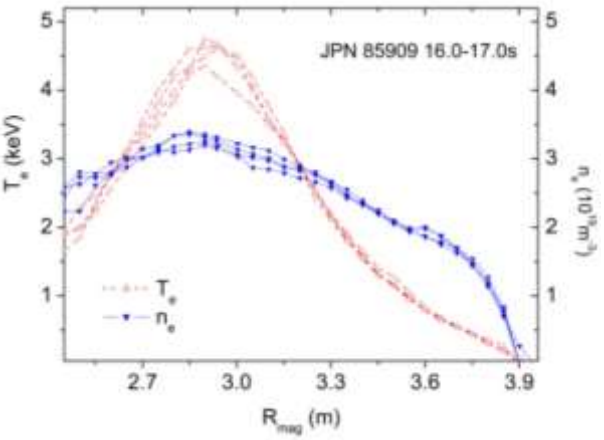

FIG. 4. Electron density and temperature profiles measured by the LIDAR Thomson scattering at JET shot #85909 in time between 16-17s.

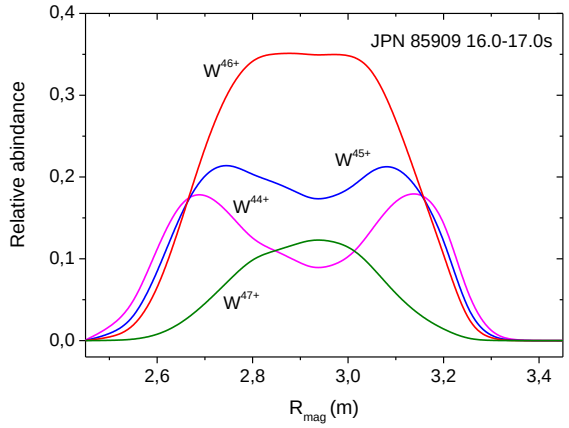

FIG. 5. Fractional abundance for W^{44+}-W^{47+}tungsten ions calculated for JET shot #85909 (time 16.0-17.0s).

Using the temperature and density profiles with ionization/recombination rates for W ions [41,42] one can estimate fractional abundance for tungsten ions. Figure 5 shows fractional abundance under ionization equilibrium (JET shot #85909, time 16.0-17.0s) for W^{44+}, W^{45+}, W^{46+} and W^{47+}ions as a function of a major radius of the line-of-sight of the KX1 JET diagnostic. It can be seen that in the core plasma W^{46+} and W^{45+} ions dominate over the other ionization stages of tungsten. The W^{46+} and W^{45+} fractional abundance increase toward the plasma core reaching the relatively broad maxima (in the case of W^{45+} ions a slightly hollow structure can be observed). Thus, one can conclude that both W^{46+} and W^{45+} x-ray lines (see Fig. 1) well represent the radiative properties of central JET plasmas.

IV. THEORETICAL CALCULATIONS

The calculations of radiative transition wavelengths were carried with the GRASP2K [43,44] and FAC [45] codes. The GRASP2K code is based on the MCDF method, and FAC on a modified Dirac-Hartree-Slater (DHS) one. The methodology of MCDF calculations performed in the present study is similar to that published earlier, in many papers (see, e.g., [46-49]). The effective Hamiltonian for an N-electron system is expressed by

$$H = \sum_{i=1}^{N} h_D(i) + \sum_{j>i=1}^{N} C_{ij}$$

where $h_D(i)$ is the Dirac operator for the ith electron and the terms C_{ij} account for electron-electron interactions. In general, the latter is a sum of the Coulomb interaction operator and the transverse Breit operator. An atomic state function (ASF) with the total angular momentum J and parity p is assumed in the form

$$\Psi_s(J^p) = \sum_m c_m(s)\Phi(\gamma_m J^p)$$

where $\Phi(\gamma_m J^p)$ are the configuration state functions (CSFs), $c_m(s)$ are the configuration mixing coefficients for state s, and γ_m represents all information required to define a certain CSF uniquely. The CSFs are linear combinations of N-electron Slater determinants which are antisymmetrized products of 4-component Dirac orbital spinors. In the present calculations, the initial and final states of considered transitions were optimized separately and the biorthonormal transformation was used [43]. Following this, the so-called relaxation effect was taken into account. In the GRASP2K code, the Breit interaction contribution to the energy was added as a perturbation, after the radial part of the wavefunction was optimized. Also two types of quantum electrodynamics (QED) corrections, self-energy (as screened hydrogenic approximation [50] of data of Mohr and co-workers [51]) and vacuum polarization (as potential of Fullerton an Rinker [52]), were included.

On the whole, the multiconfiguration DHS method is similar to the MCDF method, referring to effective Hamiltonian and multiconfigurational ASF, but a simplified expression for the electronic exchange integrals is used. However, the FAC code uses an improved form of the electron-electron interaction potential (see Ref. [45] for details). The Breit contribution and leading QED contributions are also included in FAC calculations.

The accuracy of the wavefunction depends on the CSFs included in its expansion [53,54]. The accuracy can be improved by extending the CSF set by including the CSFs originated by excitations from orbitals occupied in the reference CSFs to unfilled orbitals of the active orbital set (i.e. CSFs for virtual excited states). The CI method

makes it possible to include the major part of the electron correlation contribution to the energy of the atomic levels. The CI approach requires the choice of a proper basis of CSFs for the virtual excited states. It is reached by systematic building of CSF sequences by extending the Active Space (AS) of orbitals and monitoring concurrently the convergence of self-consistent calculations [18,53,55]. In the present work the large-scale MCDF-CI calculations were performed in order to provide high-accuracy theoretical predictions of Ni-(W^{46+}) and Cu-like (W^{45+}) line wavelength in the 5.19–5.26 Å region.

Table III. Numbers of CSFs for different active spaces used in calculations of considered transitions in Ni- and Cu-like tungsten ions.

Active space / Model	Number of CSFs (reduced)	
	upper states	lower state
W^{46+}		
Ref.	3	1
AS1	8845	302
AS2	58344	1417
AS3	152800	3370
AS4	292213	6161
W^{45+}		
Ref.	11	1
AS1	4571	77
AS2	26594	362
AS3	68624	866
AS4	130661	1589

In Table III the numbers of CSFs for different active spaces used for upper and lower states for calculations of $|[Mg]3p^5 3d^{10} 4d^1>_{J=1} \rightarrow |[Mg]3p^6 3d^{10}>_{J=0}$ transitions in Ni-like (W^{46+}) and $|[Mg]3p^5 3d^{10} 4s^1 4d^1>_{J=1/2,3/2} \rightarrow |[Mg]3p^6 3d^{10} 4s^1>_{J=1/2}$ transitions in Cu-like (W^{45+}) tungsten ions are presented. Some CSFs are excluded by using *jjreduce3* program, a part of GRASP2K program set. In this way the number of CSFs was reduced by up to 35%. The reference "Ref." configurations represent the $[Mg]3p^5 3d^{10} 4d^1$ upper and $[Mg]3p^6 3d^{10}$ lower states of transitions in W^{46+} ion and $[Mg]3p^5 3d^{10} 4s^1 4d^1$ upper and $[Mg]3p^6 3d^{10} 4s^1$ lower states of transitions in W^{45+} ion.

In Table IV the theoretical wavelengths of the Ni1, Ni2, Cu1, Cu2, and Cu3 lines are listed for the following extensions of our calculations. In the first step we have calculated the wavelengths by means of the pure Dirac-Fock approach followed by Breit and QED corrections (the first three rows in Table IV). The Breit and QED contributions shift the considered tungsten lines by about 10 mÅ (Breit) and 1mÅ (QED), respectively.

In the present paper the following active spaces of virtual orbitals were taken into account: AS1 containing subshells with n = 4 and l = 0-3, AS2 for subshells with n = 4-5 and l = 0-4, AS3 for subshells with n = 4-6 and l = 0-4, and AS4 for subshells with n = 4-7 and l = 0-4. For W^{46+} we have considered all possible single (S) and double (D) substitutions from *3s, 3p, 3d, 4d* occupied subshells. In this case the inactive core contains 1s, 2s, 2p. Because the size of expansions increases with the size of the reference set, for W^{45+} we used another model, which is a common approach (see e.g. [18,56]). The occupied subshells were divided into three kinds: inactive core, active core (C), and valence (V) subshells. All open subshells (i.e. *3p*, *4s*, and *4d* for upper states of transitions and *4s* for lower state) are considered as valence subshells. The n=1,2 subshells are an inactive core and the n=3 subshells are an active core. Then, for W^{45+} we considered SD substitutions divided into two groups: VV (both substituted electrons are from valence subshells) and CV (first substituted electron is from valence subshell and the other is from active core subshell) substitutions.

Table IV. Wavelengths for the transitions in Cu-like (W^{45+}) and Ni-like (W^{46+}) from different theoretical approaches.

		Wavelength [Å]				
		Ni1	Ni2	Cu1	Cu2	Cu3
DF		5.1831	5.2383	5.2067	5.2091	5.2191
+Breit		5.1938	5.2476	5.2170	5.2198	5.2299
+QED		5.1947	5.2486	5.2178	5.2207	5.2308
+CI:	AS1	5.1698	5.2224	5.2207	5.2242	5.2326
	AS2	5.1959	5.2484	5.2214	5.2246	5.2333
	AS3	5.1994	5.2518	5.2246	5.2276	5.2365
	AS4	5.1994	5.2517	5.2251	5.2280	5.2370

As it was described above, the correlation effects were included by taking into consideration single and double (SD) electron replacements within an active set of virtual orbitals (with restricted number of CSFs for Cu-like open shell configurations). The wavelengths calculated in the extension within the active set up to n=7 are higher from the reference values (DF+Breit+QED) by 2.3-4.7 mÅ. For this theoretical approach a good convergence was obtained for both Cu- and Ni-like ions.

V. RESULTS AND DISCUSSION

As it is shown in Section II, we have studied four EBIT spectra of W ions at the wavelength range from 5.19 Å to 5.26 Å for electron beam energies from 3.16 to 4.55 keV. In the spectra for these electron beam energies, the ground states transitions from $3p^5 3d^{10} 4s4d$ states of W^{45+} and $3p^5 3d^{10} 4d$ ones of W^{46+} ions appeared (see Fig. 2). For all considered electron beam energies, the Ni1 ($4d_{5/2} \rightarrow 3p_{3/2}$) transition dominates over the others (Cu1,2,3 and Ni2). The relative contribution from the radiation emitted by Cu-like W^{45+} ions decreases with the increase of the electron beam energy because of the lower ionization potential of Cu-like tungsten W^{45+} (2.43 keV) in comparison with Ni-like tungsten (4.06 keV) [5].

After the line identification it was possible to perform the wavelength calibration. In the first step we have applied the relative calibration based on NIST values [16,22] for Cu-like and Ni-like transitions (see Table VII). From the comparison with our MCDF-CI calculations (AS4 in Table IV) we have estimated the relative spectrometer accuracy to be 0.3 mÅ. For the absolute calibration we used the $3p_{3/2}$-1s and $3p_{1/2}$-1s lines of H-like Si (5.21677(5) Å and 5.21791(5) Å). From the comparison of our calculations with the others [57] the uncertainty of the reference wavelength was found to be accurate to 0.05 mÅ.

TABLE VII. Wavelength ground state transitions in $W^{45+,46+}$ at 5.19-5.26 Å wavelength range.

Line	Theory					Expt.		NIST[N/K]
	MCDF	MCDF-CI	FAC	RELAC[F]	COWAN[N]	Present EBIT	Other	
Ni1	5.1947[*] 5.1942[D]	5.1994[*]	5.1959[*] 5.1963[C2]	5.1944	5.218	5.2007(3)[*]	5.2002(9)[C1] 5.203 (3)[R] 5.203(3)[T] 5.199(9)[O] 5.2005(8)[JET*]	5.2004(9)
Cu1	5.2179[*]	5.2251[*]	5.2191[*] 5.2197[C2]			5.2259(4)[*]	5.2263(8)[JET*]	
Cu2	5.2207[*]	5.2280[*]	5.2218[*] 5.2230[C2]	5.2192	5.230	5.2291 (3)[*]	5.2295(8)[JET*]	5.2289(11)
Cu3	5.2308[*]	5.2370[*]	5.2316[*] 5.2313[C2]	5.2298	5.241	5.2369(3)[*]	5.238(9)[O]	5.2379(17)
Ni2	5.2486[*] 5.2472[D]	5.2517[*]	5.2500[*] 5.2495[C2]		5.272	5.2540(3)[*]	5.2520(16)[C1] 5.255(3)[T]	5.2533(9)

[*]This work,
[N]Neill et al. [16]
[K]Kramida [22]
Dong et al. [26]
[F]Fournier [27]
[C1]Clementson et al. [60]
[C2]Clementson et al. [29]
[R]Ralchenko et al. [3]
[T]Tragin et al. [61]
[O]Osborne et al. [62]

Table V. Wavelengths (λ_{expt}) of the Ni-like lines measured for various electron energies (E_e) and average values (λ_{av}).

	λ_{expt} (Å) at E_e (keV)				
Line	3.16	3.76	4.34	4.55	λ_{av}
Ni1	5.20072	5.20072	5.20071	5.20066	5.2007(3)
Ni2	5.25398	5.25399	5.25399	5.25391	5.2540(3)
Errors					
Statistics		<0.03 mÅ			
Spectrometer calib.		0.30 mÅ			
Reference		0.05 mÅ			
Ref. statistics		<0.03 mÅ			

Table VI. Wavelengths (λ_{expt}) of the Cu-like lines measured for various electron energies (E_e) and average values (λ_{av}).

	λ_{expt} (Å) at E_e (keV)				
Line	3.16	3.76	4.34	4.55	λ_{av}
Cu1	5.22590	5.22587	5.22585	5.22597	5.2259(4)
Cu2	5.22908	5.22908	5.22914	5.22921	5.2291(3)
Cu3	5.23692	5.23691	5.23684	5.23691	5.2369(3)
Errors					
Statistics Cu1		<0.20 mÅ			
Statistics Cu2,3		<0.10 mÅ			
Spectrometer calib.		0.30 mÅ			
Reference		0.05 mÅ			
Ref. statistics		< 0.03 mÅ			

The measured wavelengths of the Ni1, Ni2, Cu1, Cu2 and Cu3 lines are listed in tables V and VI together with error contributions for all spectra (3.16 keV, 3.76 keV, 4.34 keV and 4.55 keV). The wavelengths of Cu- and Ni-like tungsten lines were determined by means of multi-peak Gaussian function fits with a linear background. The determined line wavelengths from all beam energies were averaged and are presented in the last column of tables V and VI and in table VII with total errors of 0.3-0.4 mÅ. In comparison with NIST experimental values [16,22] the experimental errors were reduced at least by factor of 3 (see Table VII). To the best of our knowledge, it is the most accurate measurement in this wavelength range presented so far for Cu- and Ni-like tungsten ions. Moreover, the wavelength of Cu1 line ($3p^5 3d^{10} 4s4d\ (3/2,2)_{3/2}$ - $3d^{10}4s\ ^2S_{1/2}$) was measured for the first time. One can see in tables V and VI that the dominant contribution to the measured uncertainties originates from the relative spectrometer calibration. The crystal dispersion errors, determined with the XOP code [58], are negligible in comparison with the reference and statistics ones.

In table VII we present the experimental wavelengths of the Ni1 and Cu1,2 tungsten lines determined from JET measurements performed from the upgraded high-resolution x-ray diagnostic $\lambda/\Delta\lambda>1.2x10^4$ [32-34]. The wavelengths were determined as average values from spectra taken from plasma JET shot #85909 at 1s time intervals in time between 10-17s. The JET spectra were also fitted by multi-peak Gaussian functions with a linear background. The JET spectra can be affected by the Doppler shift due to the tokamak toroidal rotation. For the ICRF-heated JET plasmas toroidal rotation should not exceed ~20 krad s^{-1} [59] that corresponds to about 0.35 mÅ tungsten wavelength shift.

In order to calibrate JET spectra we have assumed the same toroidal rotation for tungsten and molybdenum ions and performed the wavelength calibration by means of the E1 and M2 lines of Mo^{32+} (5.2076 Å and 5.2162 Å) originating from the molybdenum impurity in JET plasmas [7,32]. The calibration wavelengths of Mo^{32+} lines were calculated by MCDF-CI method. The wavelengths of Ni1 and Cu1,2 tungsten lines determined from JET spectra are presented in table VII with total errors of 0.8 mÅ. The main contribution to the total error estimate comes from the Doppler shift correction (with 0.35 mÅ uncertainty) and the E1 and M2 Mo^{32+} reference wavelengths (0.7 mÅ). One can clearly see that the wavelengths measured at JET are in an excellent agreement (~0.3-0.5 mÅ) with values measured in the EBIT.

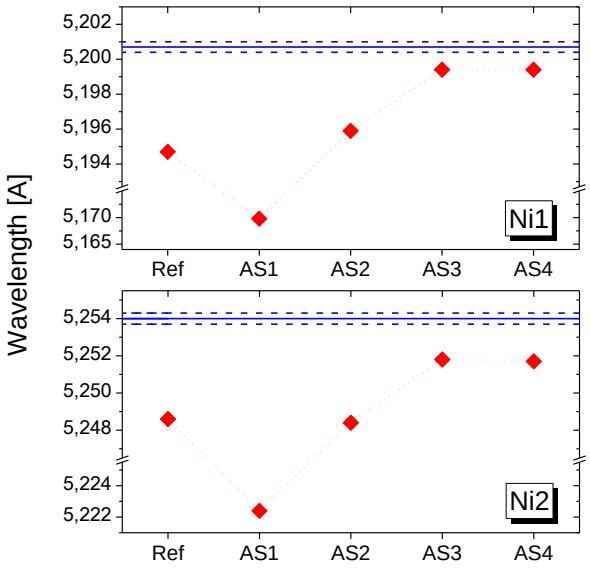

FIG. 6. The MCDF-CI wavelength calculations for Ni1 (upper) and Ni2 (bottom) tungsten lines as a function of active set (AS_n) compared to the experimental values. The dotted lines with (♦) symbols represent the MCDF-CI calculations, while solid and dashed lines show the experimental values and their uncertainties.

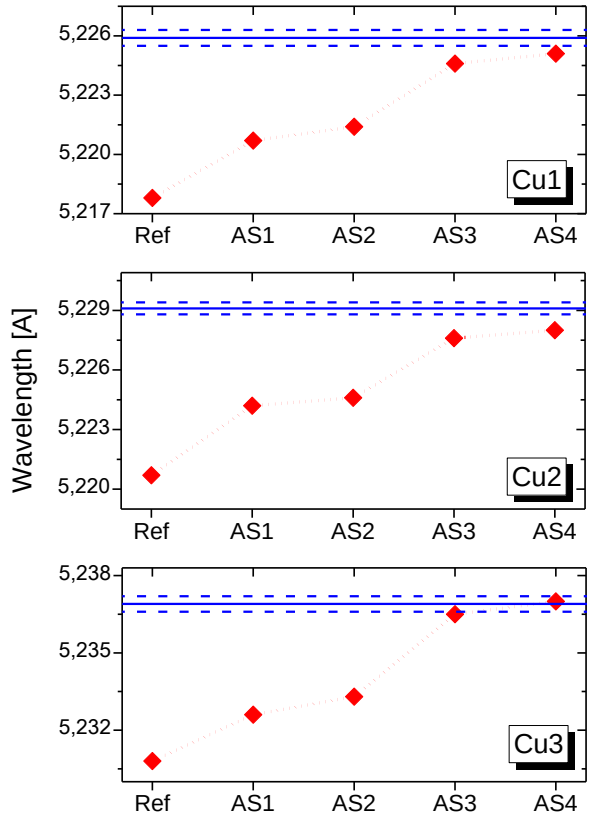

FIG. 7. Same as Fig. 6 but for Cu1, Cu2 and Cu3 tungsten lines.

In table VII the experimental wavelengths are compared with the reference MCDF, MCDF-CI, FAC, RELAC and COWAN theoretical predictions. The reference MCDF, FAC and RELAC calculations based on the fully relativistic approach agree much better with experiment than those obtained by COWAN code. This observation is consistent with that presented in other studies (see e.g. Ref. [16]).

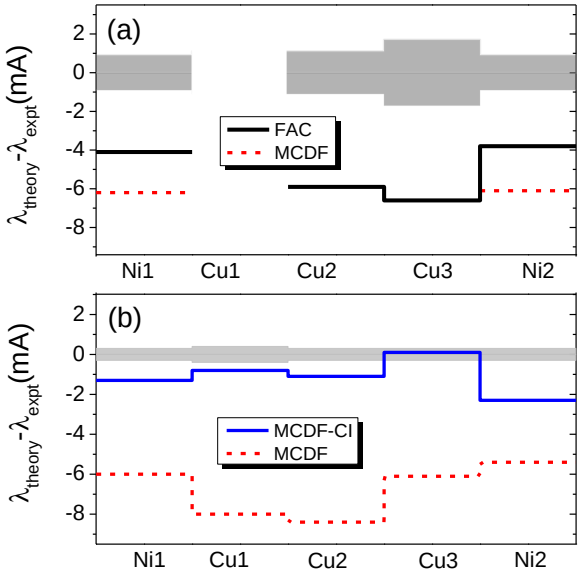

FIG. 8. Comparison of previous (a) and present (b) theoretical and experimental wavelengths of Ni1,2 and Cu1,2,3 lines. The previous experimental wavelengths are taken from Refs. [16,22], while theoretical ones from Refs. [26,29]. The experimental uncertainties are represented by shaded area.

The differences between the theoretical and experimental wavelengths of Ni- and Cu-like lines are in range of 4-10 mÅ when just the participating configurations are considered in the calculation. In order to reproduce the experimental wavelengths more accurately, we applied the high-accuracy MCDF-CI calculations taking into account the correlations effects by implementing single and double virtual excitations from the core and valence shells. Details of the method are presented in Section III. Figures 6 and 7 show the convergence behavior of theoretical predictions for Ni1,2 and Cu1,2,3 line wavelengths as a function of active set (AS_n) together with the experimental values. It is worth mentioning that for the AS1 active set containing virtual excitations to subshells with n = 4 and l = 0-3 one can observe a significant drop of the calculated wavelengths to ~5.17 Å and ~5.22 Å for Ni1 and Ni2 wavelengths, respectively (see Fig. 6). The calculations for the active sets with a higher n quantum number in the active set (and higher N_{CSF} number of CSFs) show a significant increase of the wavelengths toward experimental values of Cu1,2,3 and Ni1,2 lines. An increase of the wavelength values within AS_3 and AS_4 active sets is about 3-7 mÅ in comparison with the reference values. A convergence is reached from since the AS_3 active set (n=6) for both Cu- and Ni-like tungsten calculations..

An improvement of the experimental precision and theoretical predictions taking into account correlation effects is illustrated in Figure 8. A significant underestimation of previous experimental Cu2,3 and Ni1,2 wavelengths by MCDF and FAC theoretical predictions is shown in Fig. 8(a). Fig. 8(b) clearly

shows not only an improvement of the experimental wavelength precision (to 0.3-0.4 mÅ uncertainty values), but also presents a much better agreement between our theoretical predictions and new experimental results. The most accurate MCDF-CI calculations (with quantum number up to n=7) reduce the discrepancies between theory and experiment below 1.5 mÅ and 2.5 mÅ for Ni1, Cu1,2,3 and Ni2, respectively.

VI. SUMMARY

The high-resolution measurements of Cu- and Ni-like tungsten wavelengths were performed in the 5.19–5.26 Å range at the upgraded Shanghai-EBIT. Spectra were produced by an electron beam with energies from 3.16 keV to 4.55 keV. The Cu- and Ni-like tungsten lines were measured with a significantly better precision (0.3-0.4 mÅ) in comparison with previous ones (0.9-1.7 mÅ). Moreover, the wavelength of the ground states transition in Cu-like tungsten from the $3p^5 3d^{10} 4s4d\ [(3/2,(1/2,5/2)_2]_{1/2}$ level (Cu1 line) was measured for the first time.

The measurements were performed in the spectral range that is relevant to tokamak plasma diagnostics, in particular to the high-resolution x-ray diagnostic operated at JET. The Ni-like and Cu-like wavelengths determined from JET spectra are in an excellent agreement (~0.3-0.5 mÅ) with values measured at the Shanghai-EBIT.

It was also shown that previous calculations significantly underestimate the experimental values of Cu- and Ni-like tungsten wavelengths in the considered spectral range. Our extended MCDF calculations taking into account the correlation effects within an active set with quantum number up to $n=7$ reduce the underestimation below 2 mÅ level. Results of this study provide an important benchmark for x-ray measurements in tokamaks, in particular for JET and ITER.

ACKNOWLEDGMENTS

This work was supported by the National Magnetic Confinement Fusion Program of China with Grant No. 2015GB117000 and by the National Natural Science Foundation of China No. 11374061. The work was partly supported by the Polish Ministry of Science and Higher Education within the framework of the scientific financial resources in the years 2016-2017 allocated for the realization of the international co-financed project. This work has been carried out within the framework of the EUROfusion Consortium and has received funding from the Euratom research and training programme 2014–2018 under grant agreement No 633053. The views and opinions expressed herein do not necessarily reflect those of the European Commission.

[1] J.D. Gillaspy, J. Inst. 5, C10005 (2010).
[2] Y. Podpaly, J. Clementson, P. Beiersdorfer, J.Williamson, G. V. Brown, and M. F. Gu, Phys. Rev. A 80, 052504 (2009).
[3] Yu. Ralchenko, J. N. Tan, J. D. Gillaspy, J. M. Pomeroy, and E. Silver, Phys. Rev. A 74, 042514 (2006).
[4] D. J. Fields, R. S. Walling, G. M. Shimkaveg, B. J. MacGowan, L. B. Da Silva, J. H. Scofield, A. L. Osterheld, T. W. Phillips, M. D. Rosen, D. L. Matthews, W. H. Goldstein, and R. E. Stewart, Phys. Rev. A 46, 1606 (1992).
[5] S. R. Elliott, P. Beiersdorfer, B. J. MacGowan, and J. Nilsen Phys. Rev. A 52, 2689 (1995).
[6] P Beiersdorfer, Clementson, J Dunn, M F Gu, K Morris, Y Podpaly, E Wang, M Bitter, R Feder, KW Hill, D Johnson and R Barnsley, J. Phys. B 43 (2010) 144008.
[7] T. Nakano et al., J. Phys. B 48, 144023 (2015).
[8] K. W. Hill, M. L. Bitter, S. D. Scott, A. Ince-Cushman, M. Reinke, J. E. Rice, P. Beiersdorfer, M.-F. Gu, S. G. Lee, Ch. Broennimann, and E. F. Eikenberry, Rev. Sci. Instrum. 79, 10E320 (2008).
[9] A. Czarnecka, K.-D. Zastrow, J. Rzadkiewicz, I. H. Coffey, K. D. Lawson, M. G. O'Mullane and JET-EFDA Contributors, Plasma Phys. Control. Fusion 53, 035009 (2011).
[10] C.H. Skinner, Phys. Scr. T134 (2009) 014022.
[11] Y. Podpaly, J. Clementson, P. Beiersdorfer, J.Williamson, G. V. Brown, and M. F. Gu, Phys. Rev. A 80, 052504 (2009).
[12] C. Biedermann, R. Radtke, R. Seidel, and T. Pütterich, Phys. Scr., T 134, 014026 (2009).
[13] Ralchenko JPB 2008.
[14] J. Clementson and P. Beiersdorfer, Phys. Rev. A 81, 052509 (2010).
[15] P. Beiersdorfer, J. K. Lepson, M. B. Schneider, and M. P. Bode, Phys. Rev. A 86, 012509 (2012).
[16] P. Neill, C. Harris, A.S. Safronova, S. Hamasha, S. Hansen, U.I. Safronova, and P. Beiersdorfer, Can. J. Phys. 82, 931 (2004).
[17] Harte C S et al 2010 J. Phys. B: At. Mol. Opt. Phys. 43, 205004 (2010).
[18] Z. Fei, R. Zhao, Z. Shi, J. Xiao, M. Qiu, J. Grumer, M. Andersson, T. Brage, R. Hutton, and Y. Zou, Phys. Rev. A 86, 062501 (2012).
[19] J Clementson, P Beiersdorfer, E. W. Magee, H. S. McLean and R. D.Wood J. Phys. B: At. Mol. Opt. Phys. 43 144009 (2010).
[20] T. Putterich et al., Plasma Phys. Control. Fusion 50, 085016 (2008).
[21] J Yanagibayashi, T Nakano, A Iwamae, H Kubo, M Hasuo and K Itami, J. Phys. B: At. Mol. Opt. Phys. 43 144013 (2010).
[22] A. Kramida, Can. J. Phys. 89 (2011) 551.
[23] X.-B. Ding, F. Koike, I. Murakami, D. Kato, H.A. Sakaue, C.-Z. Dong, N. Nakamura, A. Komatsu, J. Sakoda, J. Phys. B, At. Mol. Opt. Phys. 44(14) (2011) 145004.
[24] G. Gaigalas, Z. Rudzikas, E. Gaidamauskas, P. Rynkun, A. Alkauskas, , Phys. Rev. A 82 (2010) 014502.
[25] G. Gaigalas, Z. Rudzikas, P. Rynkun, A. Alkauskas, Phys. Rev. A 83 (2011) 032509.
[26] C.Z. Dong, S. Fritzsche, L.Y. Xie, J. Quant. Spectr. Rad. Transfer 76 (2003) 447.
[27] K.B. Fournier, At. Data Nucl. Data Tables 68 (1998) 48.
[28] A.E. Kramida, T. Shirai, At. Data Nucl. Data Tables 95 (2009) 305.
[29] J. Clementson et al., At. Data Nucl. Data Tables 100 (2014) 577.

[30] F. Romanelli and JET EFDA Contributors Nucl. Fusion 53 104002 (2013).
[31] G. F. Matthews et al., Phys. Scr. T128, 137 (2007).
[32] K. Słabkowska, J. Rzadkiewicz, Ł.Syrocki, E. Szymańska, A. Shumack, M. Polasik and N.R. Pereira and JET contributors J. Phys. B: At. Mol. Opt. Phys. 49 205002 (2016).
[33] K. Słabkowska, M. Polasik, E. Szymańska, J. Starosta, Ł.Syrocki, J. Rzadkiewicz and N.R. Pereira Phys. Scr. T161 (2014) 014015.
[34] D. Lu, Y. Yang, J. Xiao, Y. Shen, Y. Fu, B. Wei, K. Yao, R. Hutton and Y. Zou, Rev. Sci. Instrum. 85, 093301 (2014).
[35] Y.Yang, D. Lu, Y. Fu, K. Yao, W. Chen, J. Xiao, Z. Geng, R. Hutton, and Y. Zou, Chin. Phys. 20, 080701(2011).
[36] x-ray Data Booklet, Section 4.1, James H. Underwood, CXRO-LBNL website.
[37] J. Rzadkiewicz et al., Nucl. Instrum. Methods Phys. Res. A 720 36 (2013).
[38] M. Chernyshova et al., JINST 9 C03003 (2014).
[39] A. E. Shumack et al., Rev. Sci. Instrum. 85 11E425 (2014).
[40] Gowers C et al 1995 Rev. Sci. Instrum. 66 471.
[41] Summers H P 2004 The ADAS User Manual version 2.6 www.adas.ac.uk.
[42] Pütterich T, Neu R, Dux R, Whiteford A D and O'Mullane M G (the ASDEX Upgrade Team) 2008 Plasma Phys. Control. Fusion 50 085016.
[43] P. Jönsson, X. He, C. Froese Fischer, and I. P. Grant, Comput. Phys. Commun. 177, 597 (2007).
[44] P. Jönsson, G. Gaigalas, J. Bieroń, C. Froese Fischer, and I. P. Grant, Comput. Phys. Commun. 184, 2197 (2013).
[45] M. F. Gu, Can. J. Phys. 86, 675 (2008).
[46] K. G. Dyall, I. P. Grant, C. T. Johnson, F. A. Parpia, and E. P. Plummer, Comput. Phys. Commun. 55, 425 (1989).
[47] I. P. Grant, Relativistic Quantum Theory of Atoms and Molecules (Springer, New York, NY, 2007).
[48] M. Polasik, K. Słabkowska, J. Rzadkiewicz, K. Kozioł, J.Starosta, E. Wiatrowska-Kozioł, J.-Cl. Dousse, and J. Hoszowska, Phys. Rev. Lett. 107, 073001 (2011).
[49] K. Kozioł and J. Rzadkiewicz, Phys. Rev. A 96, 031402(R), (2017).
[50] B. J. McKenzie, I. P. Grant, and P. H. Norrington, Comput. Phys. Commun. 21, 233 (1980).
[51] P. J. Mohr and Y.-K. Kim, Phys. Rev. A 45, 2727 (1992).
[52] L. W. Fullerton and G. A. Rinker, Phys. Rev. A 13, 1283 (1976).
[53] C. Froese Fischer, J. Phys. B At. Mol. Opt. Phys. 43, 74020 (2010).
[54] C. Froese Fischer, J. Phys. B At. Mol. Opt. Phys. 44, 125001 (2011).
[55] J. A. Lowe, C. T. Chantler, and I. P. Grant, Phys. Lett. Sect. A Gen. At. Solid State Phys. 374, 4756 (2010).
[56] C. Froese Fischer, in Adv. Theory At. Mol. Syst., edited by P. Piecuch, J. Maruani, G. Delgado-Barrio, and S. Wilson (Springer Netherlands, Dordrecht, 2009), pp. 115–128.
[57] K. M. Aggarwal and F. P. Keenan Phys. Scr. 82 065302 (2010).
[58] M. Sanchez del Rio, C. Ferrero, and V. Mocella, Proc. SPIE 3151, 312 (1997).
[59] L-G Eriksson et al., 1997
[60] J. Clementson, P. Beiersdorfer, G.V. Brown, M.F. Gu, Phys. Scr. 81 (2010) 015301.
[61] N. Tragin, J.P. Geindre, P. Monier, J.C. Gauthier, C. Chenais-Popovics, J.F. Wyart, C. Bauche-Arnoult, Phys. Scr. 37 (1988) 72.
[62] G.C. Osborne, A.S. Safronova, V.L. Kantsyrev, U.I. Safronova, P. Beiersdorfer, K.M. Williamson, M.E. Weller, and I. Shrestha, Can. J. Phys 89 (2011) 599.